Eur. Phys. J. B **1**, 197–204 (1998)

THE EUROPEAN PHYSICAL JOURNAL B

© EDP Sciences
Springer-Verlag 1998

Boundary condition histograms for modulated phases

M. Benakli[1], M. Gabay[2,a], and W.M. Saslow[3]

[1] Department of Physics, Condensed Matter Section, ICTP, P.O. Box 586, 34014, Trieste, Italy
[2] Laboratoire de Physique des Solides Laboratoire associé au CNRS, Université de Paris-Sud, Bâtiment 510, 91405 Orsay Cedex, France
[3] Department of Physics Texas A&M University College Station, Texas 77843-4242, USA

Received: 9 September 1997 / Revised: 17 October 1997 / Accepted: 3 November 1997

Abstract. Boundary conditions strongly affect the results of numerical computations for finite size inhomogeneous or incommensurate structures. We present a method which allows to deal with this problem, both for ground state and for critical properties: it combines fluctuating boundary conditions and specific histogram techniques. Our approach concerns classical systems possessing a continuous symmetry as well as quantum systems. In particular, current-current correlation functions, which probe large scale coherence of the states, can be accurately evaluated. We illustrate our method on a frustrated two dimensional XY model.

PACS. 75.10.Hk Classical spin models

Owing to their speed and power, computers are nowadays considered as experimental tools in condensed matter physics. One of their limitations stems from the fact that they can only model finite size systems and it is a drawback in some cases: for instance, in the study of critical phenomena one needs to take the infinite size limit. To overcome this problem one may specify boundary conditions (BC). One of the most common BC consist in imposing periodic boundary conditions (PBC). Unfortunately PBC may lead to numerical errors and to frustration effects. For classical Hamiltonians on a lattice this is the case when incommensurate ground states are favored or when interactions are long range [1,2]. Dipolar magnets fall into that latter class: surface contributions to the energy of the system lead to inhomogeneous structures [3,4]. For quantum systems, current carrying states are affected by boundaries (*e.g.* in mesoscopic rings [5]). The purpose of this work is to present a method designed to handle numerically systems possessing a continuous symmetry and sensitive to boundary effects. It combines self-determined (fluctuating) boundary conditions (FBC) [6,7] and specific histogram techniques. The latter feature allows to study both the ground state and the critical regime of inhomogeneous or incommensurate structures. In particular current-current correlation functions are obtained straightforwardly and the method lends itself easily to correction to scaling analysis in the critical regime. For the sake of simplicity, the main characteristics of the boundary condition histogram technique are presented for classical XY spins on a D dimensional lattice of linear size L. The validity of our approach goes beyond XY systems, and it concerns the quantum case as well.

We begin with an analytic derivation of the method; starting with the fluctuating boundary ensemble, we introduce observables. This approach is the basis of a numerical study of incommensurate phases, including the case when the modulation varies with external parameters. However, near commensurate-incommensurate transitions or in the case of inhomogeneous ground states, large numerical errors occur. We then introduce a specific histogram technique (appropriate for the fluctuating boundary ensemble) and we show how it can be used to probe the nature of equilibrium states and to gain access to thermodynamic quantities such as current-current correlation functions, including in the critical regime. Next we illustrate the features of the boundary histogram technique on the row model [8–10], a frustrated anisotropic 2D XY model: indeed, for some anisotropy range, the state of the system evolves from an incommensurate state to an inhomogeneous phase upon raising the temperature.

1 Analytic approach

We consider two components (XY) spins $\mathbf{S}(i)$ on a D dimensional lattice of linear size L. PBC impose an L-periodicity to the system:

$$\mathbf{S}(i_1,..,i_j+L,...,i_D)=\mathbf{S}(i_1,..,i_j,...,i_D);\quad \forall(i_1,..,i_j,...,i_D). \tag{1}$$

As mentioned earlier, when the spins want to form an incommensurate structure, PBC generate frustration and

[a] e-mail: marc@classic.lps.u-psud.fr

introduce systematic numerical errors. Also, inasmuch as the pitch of the spiral may vary with T and other parameters, these BC have to smoothly evolve when one changes external parameters like the anisotropies or the temperature [11].

(Self-consistent) Fluctuating Boundary Conditions have been proposed to overcome these problems [6,7]. The main feature of FBC is to add new dynamical variables Δ_α ($\alpha = 1, 2, ..., D$) corresponding to a shift at the boundaries. In equilibrium the new "boundary variables" Δ_α will fluctuate around their *most probable value* Δ_α^0.

Variants of the FBC method have also been used to accelerate the approach to the asymptotic regime, by removing some unwanted correction to scaling [12]. This improvement applies both to ferromagnetic and non-ferromagnetic systems.

1.1 Fluctuating boundary conditions

The partition function of an L^D system of XY spins with PBC is:

$$Z_{\rm PBC} = \int ... \int_{-\pi}^{\pi} \prod_i {\rm d}\Phi_i \ {\rm e}^{-\beta\left(-\frac{1}{2}\sum_{i,j} J_{ij}\cos(\Phi_i - \Phi_j)\right)} \quad (2)$$

where the PBC are expressed by the constraint

$$\Phi(\mathbf{r} + n_1 L\mathbf{u}_1 + n_2 L\mathbf{u}_2 + ... + n_D L\mathbf{u}_D) = \Phi(\mathbf{r}) \quad (3)$$

for any set of integers $n_1, n_2, ..., n_D$. This condition can be fulfilled by putting the lattice on a torus.

The FBC method imposes instead the following constraint

$$\Phi(\mathbf{r} + n_1 L\mathbf{u}_1 + n_2 L\mathbf{u}_2 + ... + n_D L\mathbf{u}_D) = \\ = \Phi(\mathbf{r}) + n_1 L\Delta_1 + n_2 L\Delta_2 + ... + n_D L\Delta_D \quad (4)$$

where $\Delta_1, ..., \Delta_D$ are new *dynamical* degrees of freedom, corresponding to a shift at the boundaries. Note that using FBC allows us to preserve translational invariance (contrary to the free BC). Performing a change of variables

$$\Phi(\mathbf{r}) = \varphi(\mathbf{r}) + \boldsymbol{\Delta}\cdot\mathbf{r} \quad (5)$$

with $\boldsymbol{\Delta} = \Delta_1\mathbf{u}_1 + ... + \Delta_D\mathbf{u}_D$, the constraint on φ becomes

$$\varphi(\mathbf{r} + n_1 L\mathbf{u}_1 + ... + n_D L\mathbf{u}_D) = \varphi(\mathbf{r}). \quad (6)$$

In terms of the new variable φ the partition function of the L^D system with FBC is:

$$Z_{\rm FBC} = L^D \\ \times \int_{-\pi/L}^{\pi/L} {\rm d}^D\Delta \left(\int ... \int_{-\pi}^{\pi} \prod_i {\rm d}\varphi_i {\rm e}^{-\beta\left(-\frac{1}{2}\sum_{i,j} J_{ij}\cos(\varphi_i - \varphi_j + \boldsymbol{\Delta}\cdot(\mathbf{r}_i - \mathbf{r}_j))\right)} \right). \quad (7)$$

Wrapping the lattice around a torus automatically enforces the constraint (Eq. (6)). It is important to note that the integration in equation (7) is over an interval of size 2π for φ_i , whereas it is over a $2\pi/L$ interval for $\Delta_1, ..., \Delta_D$. The integration range reflects the periodicity of the Hamiltonian.

$Z_{\rm FBC}$ can be factorized as a product of a set of partition functions, $Z(\boldsymbol{\Delta})$, each one corresponding to a fixed shift $\boldsymbol{\Delta}$ at the boundaries.

$$Z_{\rm FBC} = L^D \int_{-\pi/L}^{\pi/L} Z(\boldsymbol{\Delta}) {\rm d}^D\Delta \\ = L^D \int_{-\pi/L}^{\pi/L} {\rm d}^D\Delta \ {\rm e}^{-\beta L^D f(\boldsymbol{\Delta})} \quad (8)$$

where $f(\boldsymbol{\Delta})$ is the $2\pi/L$ periodic free energy density associated with the shift $\boldsymbol{\Delta}$ at the boundary:

$$f(\boldsymbol{\Delta}) = -T\ln(Z(\boldsymbol{\Delta}))/L^D. \quad (9)$$

For $\boldsymbol{\Delta} = \mathbf{0}$, we recover the PBC case, *i.e.* $Z_{\rm PBC} = Z(\boldsymbol{\Delta} = \mathbf{0})$ and $f_{\rm PBC} = f(\boldsymbol{\Delta} = \mathbf{0})$.

1.1.1 The low temperature regime

First let us consider the case of a "ferromagnetic phase" at low temperature. The integral (Eq. (8)) is dominated by the minima of $f(\boldsymbol{\Delta})$; so here, $\boldsymbol{\Delta} = \mathbf{0}$. We are then allowed to make an expansion of the integrand around $\boldsymbol{\Delta} = \mathbf{0}$; for a lattice with inversion symmetry, we get:

$$Z_{\rm FBC} = L^D \times \\ \int_{-\pi/L}^{+\pi/L} {\rm d}^D\Delta \ {\rm e}^{\left[-\beta L^D\{f_{\rm PBC} + \frac{1}{2}\frac{\delta^2 f(\boldsymbol{\Delta})}{\delta\Delta_1^2}\Big|_0 \Delta_1^2 + ... + \frac{1}{2}\frac{\delta^2 f(\boldsymbol{\Delta})}{\delta\Delta_D^2}\Big|_0 \Delta_D^2 + O(\Delta^4)\}\right]}. \quad (10)$$

The second derivatives of the free energy are related to the components $\gamma^{11}, ..., \gamma^{DD}$ of the spin rigidity tensor $\bar{\bar{\gamma}}$ by a geometrical factor ρ

$$\gamma^{11} = \rho \left.\frac{\delta^2 f(\boldsymbol{\Delta})}{\delta\Delta_1^2}\right|_0, ..., \quad \gamma^{DD} = \rho \left.\frac{\delta^2 f(\boldsymbol{\Delta})}{\delta\Delta_D^2}\right|_0 \quad (11)$$

(*e.g.*, in 2D, ρ is 1 for the square lattice, and $2/\sqrt{3}$ for the triangular lattice).

We rewrite equation (10), after rescaling $\boldsymbol{\Delta}$, $\boldsymbol{\Delta}' = L\boldsymbol{\Delta}$:

$$Z_{\rm FBC} \simeq Z_{\rm PBC} \int_{-\pi}^{+\pi} {\rm d}^D\Delta' \exp\left[-\frac{1}{2\rho}\beta L^{D-2} \right. \\ \left. \times \left(\gamma^{11}\Delta_1'^2 + ... + \gamma^{DD}\Delta_D'^2\right) \right]. \quad (12)$$

We deduce the formal expression connecting $Z_{\rm FBC}$ and $Z_{\rm PBC}$ at low temperature, by extending the domain of integration of Δ' to $[-\infty, +\infty]$:

$$Z_{\rm FBC} = Z_{\rm PBC}\left(\frac{(2\pi\rho)^{\frac{D}{2}}}{(\beta L^{D-2})^{\frac{D}{2}}\gamma} + O(\frac{1}{\beta^{\frac{D}{2}+1}})\right) \quad (13)$$

where $\gamma = \sqrt{\gamma^{11}\cdot\gamma^{22}\cdot ...\cdot\gamma^{DD}}$.

For a system with a helical phase at low temperature, the same analysis can be repeated, leading to the expressions:

$$Z_{\rm FBC} \simeq Z(\boldsymbol{\Delta}^0) \int_{-\pi}^{+\pi} {\rm d}^D \Delta' \exp\Big[-\frac{1}{2\rho}\beta L^{D-2} \times \left(\gamma^{11}{\Delta'}_1^2 + ... + \gamma^{DD}{\Delta'}_D^2\right)\Big] \quad (14)$$

and

$$Z_{\rm FBC} = Z(\boldsymbol{\Delta}^0)\left(\frac{(2\pi\rho)^{\frac{D}{2}}}{(\beta L^{D-2})^{\frac{D}{2}}\gamma} + O(\frac{1}{\beta^{\frac{D}{2}+1}}\right) \quad (15)$$

$$\gamma^{11} = \rho\left.\frac{\delta^2 f(\boldsymbol{\Delta})}{\delta\Delta_1^2}\right|_{\boldsymbol{\Delta}^0}, ..., \quad \gamma^{DD} = \rho\left.\frac{\delta^2 f(\boldsymbol{\Delta})}{\delta\Delta_D^2}\right|_{\boldsymbol{\Delta}^0}. \quad (16)$$

Here $\boldsymbol{\Delta}^0$ is the minimum of $f(\boldsymbol{\Delta})$, determined *modulo* $2\pi/L$ from:

$$\left.\frac{\delta f(\boldsymbol{\Delta})}{\delta\Delta_1}\right|_{\boldsymbol{\Delta}^0} = 0 \quad , ..., \quad \left.\frac{\delta f(\boldsymbol{\Delta})}{\delta\Delta_D}\right|_{\boldsymbol{\Delta}^0} = 0. \quad (17)$$

For a spiral phase, the pitch $\mathbf{Q}_0$ is the $2\pi/L$ determination of $\boldsymbol{\Delta}^0$ such that $\varphi(\mathbf{r}) \approx 0$ in equilibrium (see Eq. (5)).

From equation (14) we deduce [6]

$$\gamma^{11} = \frac{\rho}{L^D \chi_{\Delta_1}}, ..., \quad \gamma^{DD} = \frac{\rho}{L^D \chi_{\Delta_D}} \quad (18)$$

where $\forall\alpha = 1, .., D \quad \chi_{\Delta_\alpha} = \beta\langle(\Delta_\alpha - \Delta_\alpha^0)^2\rangle$ is the susceptibility for Δ_α. The validity of equation (18) is restricted to the low temperature regime; more precisely, to the region of the phase diagram where $\forall\alpha = 1, .., D$, $\beta\gamma^{\alpha\alpha} \gg 1$.

1.1.2 Observables

Using FBC implies that thermodynamic quantities such as the energy or the spin rigidity will be different from those evaluated with PBC. From our previous discussion, this difference shows to leading order in size in the incommensurate phase but it is also present for a commensurate phase (to order $O(1/L^D)$).

For the sake of simplicity we assume in this section that $f(\boldsymbol{\Delta})$ has its minimum at $\boldsymbol{\Delta} = \mathbf{0}$. The results, however, do not depend on the particular value of $\boldsymbol{\Delta}^0$ which minimizes f.

For a given observable $O(\Phi_j)$ the values computed with PBC and with FBC are:

$$\langle O\rangle_{\rm PBC} = \frac{1}{Z_{\rm PBC}} \times \int ... \int_{-\pi}^{\pi} \prod_i {\rm d}\Phi_i O(\Phi_j) {\rm e}^{\frac{\beta}{2}\sum_{ij} J_{ij}\cos(\Phi_i - \Phi_j)} \quad (19)$$

$$\langle O\rangle_{\rm FBC} = = \frac{1}{Z_{\rm FBC}} L^D \int_{-\pi/L}^{\pi/L} {\rm d}^D\Delta \int ... \int_{-\pi}^{\pi} \prod_i {\rm d}\varphi_i O(\varphi_j + \boldsymbol{\Delta}\cdot\mathbf{r}_j) \times {\rm e}^{\frac{\beta}{2}\sum_{ij} J_{ij}\cos(\varphi_i - \varphi_j + \boldsymbol{\Delta}\cdot(\mathbf{r}_i - \mathbf{r}_j))}. \quad (20)$$

The two expressions generally differ by an $O(1/L^D)$ term: for instance the average energy density is obtained by taking the derivative of equation (15) with respect to β yielding

$$e_{\rm FBC} = e_{\rm PBC} + \frac{D/2}{\beta L^D} + O(1/\beta^2). \quad (21)$$

Studying these corrections allows us to minimize undesired finite size effects (Ref. [12]).

Since the FBC partition function (8) includes all possible BC, it is possible (at least analytically) to obtain $\langle O\rangle_{\rm PBC}$ directly from the FBC partition function:

$$\langle O\rangle_{\rm PBC} = \frac{\langle O\delta(\boldsymbol{\Delta} - \mathbf{0})\rangle_{\rm FBC}}{\langle\delta(\boldsymbol{\Delta} - \mathbf{0})\rangle_{\rm FBC}} \quad (22)$$

where $\delta(x)$ is the Dirac distribution.

For most observables, $\langle O\rangle_{\rm FBC}$ and $\langle O\rangle_{\rm PBC}$ differ solely by *corrections to scaling*. This is, however, not true for the spinwave stiffness.

Evaluating the spin rigidity using FBC is more involved: this quantity is a (spin) current-current correlation function and measures the phase coherence of the system. The standard definition of $\bar{\bar{\gamma}}$, namely the response of the system to a shift at the boundary, *trivially leads to a zero value*. This follows from the very implementation of FBC, since for any imposed shift, the dynamical variable $\boldsymbol{\Delta}$ can adapt itself to absorb the shift at no cost in free energy. We need another way to compute the spinwave stiffness. For instance, from equation (18) the spin rigidity can be computed *via* the susceptibility of $\boldsymbol{\Delta}$: one should keep in mind that this expression is only valid for $\beta\gamma^{11} \gg 1, ..., \beta\gamma^{DD} \gg 1$, because we have extended the domain of integration of Δ' to $[-\infty, +\infty]$. Near a commensurate-incommensurate boundary, at least one of the $\gamma^{\alpha\alpha} \to 0$, and so one needs to use another procedure.

Another limitation of this approach concerns inhomogeneous states: in that case one cannot use a single, constant $\boldsymbol{\Delta}$; for domains separated by domain walls, for instance, each domain wall constitutes a boundary and $\boldsymbol{\Delta}$ depends on spatial coordinates.

To overcome these problems, we will now introduce $\Delta-$histograms, in conjunction with FBC.

1.2 $\boldsymbol{\Delta}$-Histograms

In part 1.1 we showed that the partition function with FBC is a sum over partition functions $Z(\boldsymbol{\Delta})$. A practical way to perform this sum is to count the number

of configurations obtained for each of the allowed values of $\Delta_1, ..., \Delta_D$. Since these quantities are defined *modulo* $2\pi/L$, this can be easily done by histograms in $\Delta_1, ..., \Delta_D$ which we call Δ-histograms.

From the standpoint of a Monte Carlo simulation, histograms are generated as follows: we divide the range of variation of $\Delta_1, ..., \Delta_D$ into smaller sub-intervals. For each of these we store the total number of configurations $n(\boldsymbol{\Delta})$ having $\Delta_1, ..., \Delta_D$ within the given interval, and also the average of relevant quantities (such as the energy) over these configurations.

This yields the probability distribution $P(\boldsymbol{\Delta})$ for Δ, and averages $O^{\rm hist}(\boldsymbol{\Delta})$ of various observables.
$P(\boldsymbol{\Delta})$ is given by

$$P(\boldsymbol{\Delta}) = \frac{n(\boldsymbol{\Delta})}{\mathcal{N}} \tag{23}$$

where $\mathcal{N}$ is the total number of generated configurations. Similarly
$O^{\rm hist}(\boldsymbol{\Delta})$ is given by:

$$O^{\rm hist}(\boldsymbol{\Delta}) = \frac{1}{n(\boldsymbol{\Delta})} \sum_{\mathcal{C}(\boldsymbol{\Delta})} O(\mathcal{C}(\boldsymbol{\Delta})) \tag{24}$$

where $\sum_{\mathcal{C}(\boldsymbol{\Delta})}$ is the sum over all configurations having their boundary phase shift $\Delta_1, ..., \Delta_D$ in the same given histogram interval.

According to equation (8), $P(\boldsymbol{\Delta})$ in equation (23) is proportional to $\mathrm{e}^{-\beta L^D f(\boldsymbol{\Delta})}$. Thus we have direct access to the free energy dependence on $\boldsymbol{\Delta}$. A minimum of the free energy translates into a maximum in $P(\boldsymbol{\Delta})$, giving both $\boldsymbol{\Delta}^0$ (and thus $\mathbf{Q}_0$ the wavevector of the incommensurate structure, see below) and γ. If the peak in $P(\boldsymbol{\Delta})$ is sharp enough, thermodynamic quantities are computed for the most probable value of $\boldsymbol{\Delta}$; deviations are expected when $\gamma \to 0$ or when $P(\boldsymbol{\Delta})$ has a multi-peak structure.

1.3 Thermodynamics

From our previous discussion, we can extract relevant quantities from a Monte Carlo study either by using FBC without histograms, or by using FBC with histograms. This latter approach will give better results when the system is close to a phase transition. We can implement histogram techniques in our simulation in two ways.

1.3.1 Taking numerical derivatives of the Δ-histogram free energy

The Δ-histogram free energy density is obtained from:

$$f(\boldsymbol{\Delta}) = -\frac{1}{\beta L^D} \ln\left(P(\boldsymbol{\Delta})\right) + \text{Constant}. \tag{25}$$

The zeroes of the first derivative of the free energy yield the value of $\boldsymbol{\Delta}^0$. The second derivatives of the free energy computed for $\boldsymbol{\Delta} = \boldsymbol{\Delta}^0$ give the components of the spin-wave stiffness γ by equation (16). The *advantage* of this method lies in the fact that it is a fast algorithm since *no observables are computed*. Yet, taking the first and second numerical derivatives of the free energy induces additional sources of errors in the results; however this can easily be corrected by using polynomial approximations in the vicinity of $\boldsymbol{\Delta}^0$. This method is well suited for a scaling analysis.

1.3.2 Fluctuation-dissipation-like theorem with Δ-histograms

This approach is similar to the previous method, except that the explicit expressions for the needed derivatives are computed analytically: using equations (7, 8) we obtain $\forall \alpha$:

$$\left.\frac{\partial f}{\partial \Delta_\alpha}\right|_{\Delta'_\alpha} = \frac{1}{N} \left\langle B \delta_{\boldsymbol{\Delta}'} \right\rangle_{\rm FBC} \tag{26}$$

$$\left.\frac{\partial^2 f}{\partial \Delta_\alpha^2}\right|_{\Delta'_\alpha} = \frac{\rho}{N} \times \left\{ \left\langle A \delta_{\boldsymbol{\Delta}'} \right\rangle_{\rm FBC} - \frac{1}{T} \left[\left\langle B^2 \delta_{\boldsymbol{\Delta}'} \right\rangle_{\rm FBC} - \left\langle B \delta_{\boldsymbol{\Delta}'} \right\rangle_{\rm FBC}^2 \right] \right\} \tag{27}$$

where N is the total number of spins and:

$$A = \frac{1}{2} \sum_{i,j} \frac{1}{2} J_{ij} (\mathbf{u}_{ij} \cdot \boldsymbol{u}_\alpha)^2 \cos(\varphi_i - \varphi_j + \boldsymbol{\Delta} \cdot (\mathbf{r}_i - \mathbf{r}_j)) \tag{28}$$

$$B = \frac{1}{2} \sum_{i,j} J_{ij} (\mathbf{u}_{ij} \cdot \mathbf{u}_\alpha) \sin(\varphi_i - \varphi_j + \boldsymbol{\Delta} \cdot (\mathbf{r}_i - \mathbf{r}_j)) \tag{29}$$

$$\delta_{\boldsymbol{\Delta}'} = \delta\left(\boldsymbol{\Delta} - \boldsymbol{\Delta}'\right). \tag{30}$$

This allows a better determination of the two derivatives compared to the previous method but it implies a slowing down of the algorithm, due to the computation of averages.

General remarks on the Δ-histogram method

- $\boldsymbol{\Delta}^0$ measures the incommensurability of the system; since the partition function is $2\pi/L$ periodic, Δ is obtained *modulo* $2\pi/L$. Changing $\boldsymbol{\Delta}$ to $\boldsymbol{\Delta} + (2\pi/L)\mathbf{u}_\alpha$ corresponds to replacing the angular variables φ_i by $\varphi_i - (2\pi/L)\mathbf{u}_\alpha \cdot \mathbf{r}_i$ and leaves the partition function unchanged. For an homogeneous state, the helicity — denoted by $\mathbf{Q}$ — is defined *modulo* 2π. In the simulation we may identify its equilibrium value $\mathbf{Q}_0$ with the value $\boldsymbol{\Delta}^0$ corresponding to $\varphi \simeq 0$ (see Eq. (5)). Working at low T ensures that the determination of $\boldsymbol{\Delta}^0$ will not drift by increments of $2\pi/L$ (a variation of $\boldsymbol{\Delta}^0$ by $2\pi/L$ would entail a shift in φ by $(2\pi/L)\mathbf{u}_x$, which will not occur within a reasonable number of Monte Carlo steps at low T).

- According to the previous discussion, at low enough T one can construct 2π Δ-histograms: the $2\pi/L$ periodicity does not show up in the results of the simulation. Closer to the transitions, energy barriers between states separated by $2\pi/L$ become low and one needs to restrict the histogram to the relevant $2\pi/L$ interval.
- Near phase boundaries, histogram techniques allow more accurate determinations of thermodynamic quantities. Within that framework it is also possible to reduce corrections to scaling, for instance by adding an extra term of the form $\mu(\boldsymbol{\Delta} - \boldsymbol{\Delta}^0)^2$ to the partition function and thus to $P(\boldsymbol{\Delta})$, and then by determining μ self-consistently such that corrections to scaling be minimized (Ref. [12]).
- Using histograms can give information about the nature of the commensurate-incommensurate (C)-(IC) transition: in the incommensurate phase, the free energy displays two minima at $\pm\boldsymbol{\Delta}^0$. A first order transition will be characterized by the coexistence of a third local minimum in $f(\boldsymbol{\Delta})$ for $\boldsymbol{\Delta} = \mathbf{0}$, at some characteristic temperature.

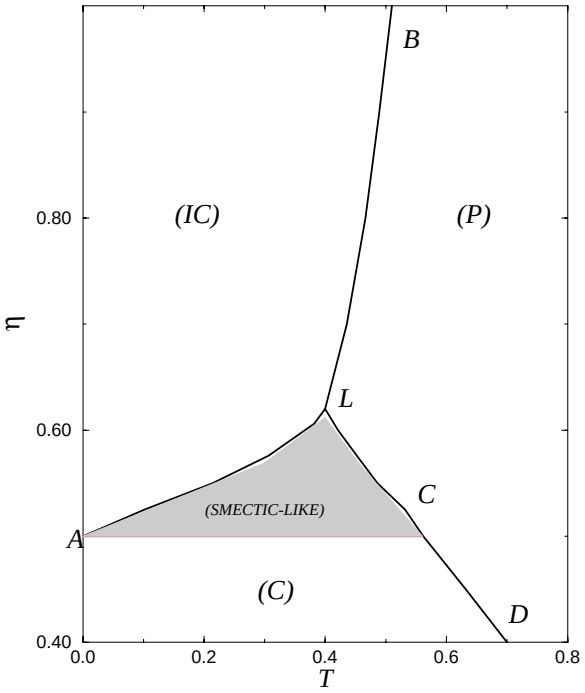

Fig. 1. MC phase diagram of the row model, in the (η, T) plane.

2 Application of the boundary condition histogram technique

In order to illustrate the main features of the method introduced in section 1, we consider the row model, a frustrated anisotropic 2D XY model defined on the triangular lattice [8–10]. Only nearest neighbor sites are coupled: $J_{ij} = -\eta J$ $(J > 0)$ for i and j along the horizontal direction and $J_{ij} = -J$ otherwise. The case $\eta = 1$ corresponds to the fully frustrated model [13] but here we will assume $\eta \neq 1$. At $T = 0$ the following phase diagram is obtained. For $\eta < 0.5$ one has a commensurate collinear antiferromagnetic phase. For $\eta > 0.5$ an incommensurate spiral state is observed in the horizontal direction denoted by x. The entire phase diagram of the row model, in the (η, T) plane, was previously studied in Monte Carlo. Since the incommensurability is only present in the x direction hybrid boundary conditions were used: PBC in the y direction and FBC *without* Δ-histograms in the x direction. Three phases were identified (see Fig. 1): a low T commensurate state (C) bounded by lines ALCD, a low T incommensurate state (IC) bounded by lines ALB and a high T paramagnetic state (P). AL is a commensurate-incommensurate transition line: starting from $T = 0$ and increasing T at fixed η, γ^{xx} — the x component of the spinwave stiffness — *computed via equation (18)*, decreases, vanishes continuously upon reaching line AL, increases again and eventually goes back to zero on the LCD boundary. For this particular thermodynamic path, Q_x, the (incommensurate) wave vector in the x direction decreases and vanishes continuously on AL.

The choice of this model stems from the fact that *(i)* as T approaches $T_{\rm AL}$ (the temperature of the (C)-(IC) transition), $\gamma^{xx} \to 0$ and thus equation (18) ceases to be valid; *(ii)* for $T > T_{\rm AL}$ the state of the system consists of a multidomain structure and is not a homogeneous (C) phase (Ref. [14] and see below): (FBC), in the original form [6,7], select $\boldsymbol{\Delta}^0$, the most probable value of $\boldsymbol{\Delta}$, whereas the inhomogeneous character of the state requires more than one $\boldsymbol{\Delta}$. Δ-histograms then prove a useful tool to study the thermodynamics of the row model in the vicinity of the (C)-(IC) transition.

In the present simulation, we used Δ-histograms. A standard Metropolis algorithm was applied to the spin angles and to the boundary shift in the x direction. We worked with a 48^2 lattice and the number of MCS/spin was of order 10^5–10^6. Typically the first 10^4 steps were discarded for equilibration. We monitored Q_x, γ^{xx}, γ^{yy} (the y component of the spinwave stiffness) and the staggered chiralities [13]. We chose $\eta = 0.55$ and varied the temperature. A detailed analysis of the simulation is presented in (Ref. [14]).

1. At low temperature, in the incommensurate phase (IC) (see Fig. 1), we can construct 2π Δ-histograms as discussed in the general remarks of section 1. The corresponding histogram for Q_x is shown in Figure 2. At a given T, $P(Q_x)$ displays two well defined peaks for $Q_x = +Q_0(T)$ and $Q_x = -Q_0(T)$ (the figure only shows positive values of Q_x). As the temperature brings the system closer to line AL, the peaks at $Q_x = +Q_0(T)$ and $Q_x = -Q_0(T)$ broaden and tend to merge. In that regime, $\boldsymbol{\Delta}^0$ drifts easily and if one still uses 2π histograms one finds that $Q_x = 0$ for $T \geq T_{\rm AL}$ (Fig. 3). On the other hand if the $2\pi/L$ periodicity of Δ_x is enforced, one finds that $P(Q_x)$ shows three peaks as a function of Q_x, for $T \geq T_{\rm AL}$ (Figs. 4, 5). The relative weight of the side peaks compared to that of the central peak ($Q_x = 0$) is roughly one: 25% of

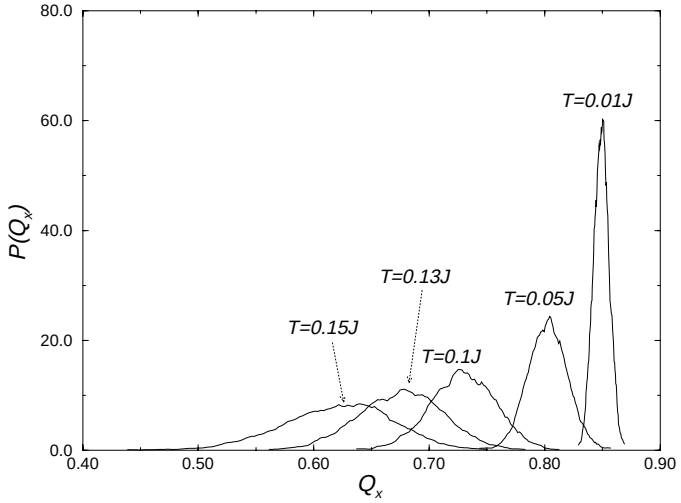

Fig. 2. Unnormalized 2π Δ-histogram $P(Q_x)$ for the wavevector Q_x at various temperatures. Only positive values of Q_x are shown, since $P(Q_x) = P(-Q_x)$.

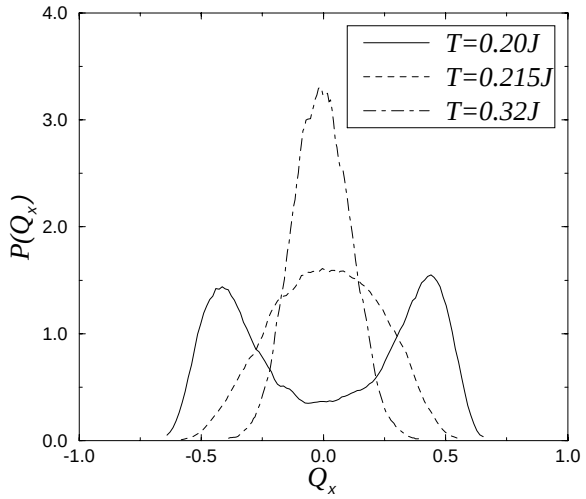

Fig. 3. Unnormalized 2π Δ-histogram $P(Q_x)$ for the wavevector Q_x at various temperatures. For $T \geq T_{\rm AL} \approx 0.19J$, $P(Q_x)$ has a single maximum at $Q_x = 0$.

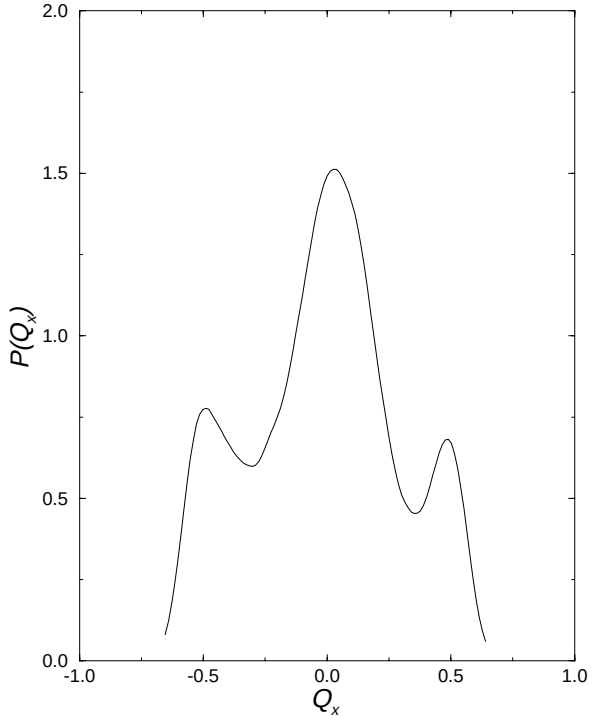

Fig. 4. Unnormalized $\frac{2\pi}{L}$ Δ-histogram $P(Q_x)$ *versus* Q_x for $\eta = 0.55$ and $T = 0.19J$.

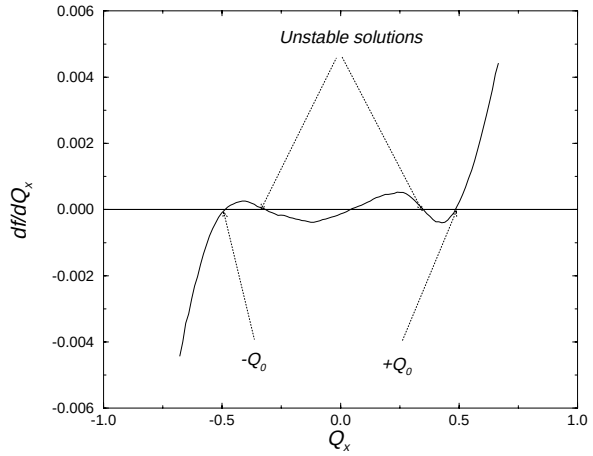

Fig. 5. First derivative of the free energy density *versus* Q_x for $\eta = 0.55$ and $T = 0.19J$.

the system is in a spiral state with wavevector $Q_x = +Q_0(T)$, 25% is in a spiral state with wavevector $Q_x = -Q_0(T)$ and 50% in a collinear state. The multi-peak structure evokes the hysteresis often present in first order transitions but in fact it is due to the existence of an inhomogeneous structure for $T \geq T_{\rm AL}$ (see below).

2. At low temperature, in the incommensurate phase (IC), the determinations of γ^{xx} *via* equation (18), *via* 2π Δ-histograms or *via* $2\pi/L$ Δ-histograms all agree (Figs. 6, 7). However for $T \geq 0.10J$ the three curves move apart. In particular, for $T \geq T_{\rm AL} \approx 0.19J$, γ^{xx} as obtained from $2\pi/L$ Δ-histograms is zero within our error bars, whereas it is positive with the other methods.
γ^{yy} does not show any singularity: it decreases as T increases and vanishes on the paramagnetic boundary (line LCD of Fig. 1).

For $T \to T_{\rm AL}$ from above, spins undergo critical fluctuations. At a given T the MC process generates fluctuations in $\boldsymbol{\Delta}^0$ by large increments of $2\pi/L$. If we use 2π Δ-histograms instead of $2\pi/L$ Δ-histograms (as one should) these fluctuations smear out the structure of the $2\pi/L$ Δ-histogram (Fig. 4). The 2π Δ-histogram (Fig. 3) yields a single peak at $Q_x = 0$: this value is the mean of Q_x averaged over the $2\pi/L$ Δ-histogram; similarly the width of the 2π Δ-histogram is of the order of the average of Q_x^2 over the $2\pi/L$ Δ-histogram.

The multi-peak structure of the $2\pi/L$ Δ-histogram also signals the breakdown of the fluctuation-dissipation theorem: computing γ^{xx} for the most probable value of

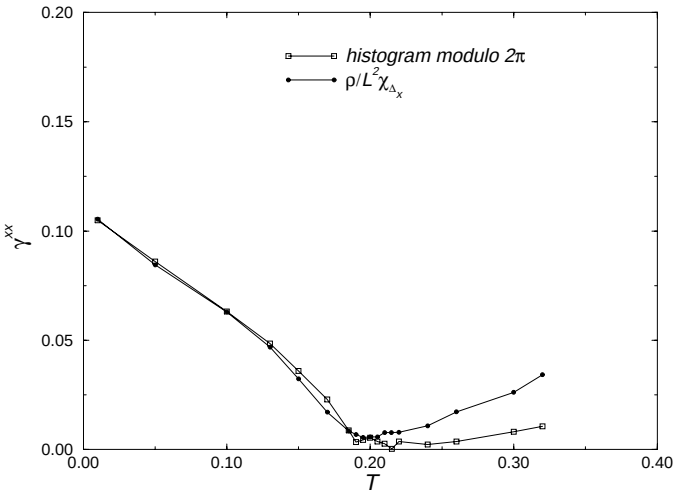

Fig. 6. Comparison of MC data for γ^{xx} using Δ-histograms *modulo* 2π or using the fluctuation-dissipation theorem (Eq.18).

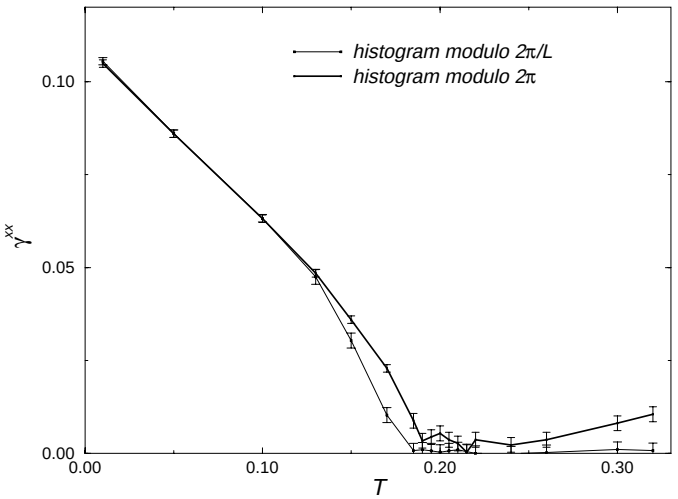

Fig. 7. Comparison of MC data for γ^{xx} using Δ-histograms *modulo* 2π or *modulo* $2\pi/L$.

Q_x (*i.e.* $Q_x = 0$) gives a larger result than that obtained *via* equation (27). The former value of γ^{xx} is comparable to what one gets *via* 2π Δ-histograms. This explains Figure 7. It also explains why γ^{xx} determined *via* the most probable value of Q_x is non zero for $T > T_{\rm AL}$.

The fact that γ^{xx} vanishes continuously at $T = T_{\rm AL}$ suggests that the commensurate-incommensurate transition is not first order. The structure of $P(Q_x)$ and the temperature dependence of γ^{xx} for $T \geq T_{\rm AL}$ signal in fact an inhomogeneous equilibrium state with striped domains in which $Q_x = +Q_0(T)$, $Q_x = -Q_0(T)$ or $Q_x = 0$ [4,14–16]. We dub this phase a smectic-like phase [17]: in this state, the elasticity in the x direction vanishes, whereas it is finite in the y direction. The Hamiltonian describing long wavelength fluctuations is smectic-like [17], *i.e.* with a momentum dependence of the inverse propagator varying as Q_x^4 for the x part and quadratically with Q_y for the y part. The structure is exhibited in a snapshot of

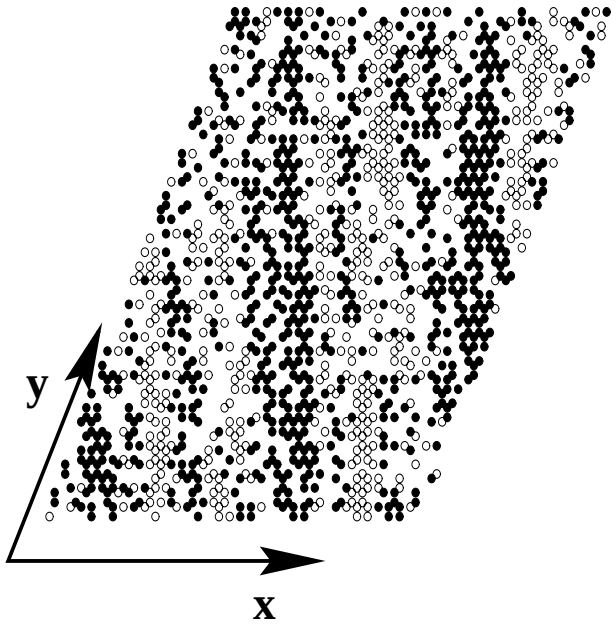

Fig. 8. Snapshot of chiralities on each plaquette of a 36^2 triangular lattice. for $T = 0.4J$. Filled circles represent plaquettes with the correct sign, i.e in the same chiral state as at $T = 0$. Open circles correspond to plaquettes with the wrong sign, that is such that the chirality has changed compared to $T = 0$. Plaquettes with zero chirality (no symbol) are obtained in-between the two. One clearly sees a stripe structure of filled circles and open circles separated by domain walls of zero chirality. The horizontal (x) axis corresponds to the direction of the η bonds.

the chiralities of the system (Fig. 8): chiralities are positive for domains having $Q_x = +Q_0(T)$, negative for domains having $Q_x = -Q_0(T)$ and zero for walls ($Q_x = 0$). At the transition, for $T = T_{\rm AL}$, the stripe structure is stabilized [2,18].

The same characteristics are observed in the entire region ALC of the phase diagram (see Fig. 1).

So, in contrast to the previous MC study, we find here four phases in the (η, T) plane. In addition to the (C), (IC) and (P) phases, an inhomogeneous thermodynamic state is observed between the (C) and (IC) phases, bounded by lines ALC (see Fig. 1). Its presence was revealed by our method.

3 Conclusion

We have presented a technique allowing to study numerically the ground state and the critical regime of finite size inhomogeneous or incommensurate structures. We illustrate its features on the commensurate-incommensurate transition of classical 2D XY spins on the triangular lattice

Monte Carlo calculations were performed on a Cray C98 thanks to contract 960162 from IDIS. Support from NATO grant 930988 is acknowledged.

References

1. H.T. Diep, *Magnetic Systems with competing interactions* (World Scientific, 1994).
2. W. Selke, in *Phase transitions and Critical Phenomena* edited by Domb and Lebowitz (Academic Press, 1992), Vol. 15, p. 2.
3. M. Gabay, T. Garel, J. Phys. France **46**, 5 (1985); Phys. Rev. **B 33**, 6281 (1986).
4. A. Kashuba, Phys. Rev. Lett. **77**, 2554 (1996).
5. *Proceedings of the Les Houches Summer School on Mesoscopic Quantum Physics, Les Houches, France, 28-29 June 1994* (Elsevier, 1995).
6. W.M. Saslow, M. Gabay, W.-M. Zhang, Phys. Rev. Lett. **68**, 3627 (1992).
7. P. Olsson, Phys. Rev. Lett. **73**, 3339 (1994).
8. W.-M. Zhang, W.M. Saslow, M. Gabay, Phys. Rev. **B 43**, 11285 (1991).
9. W.-M. Zhang, W.M. Saslow, M. Gabay, M. Benakli, Phys. Rev. **B 48**, 10204 (1993).
10. H. Kawamura, Prog. Theor. Phys. Jpn Suppl. **101**, 545 (1990).
11. H.T. Diep, Phys. Rev. **B 39**, 397 (1989); *ibid.* **B 40**, 741 (1989).
12. P. Olsson, Phys. Rev. **B 52**, 4511 (1995).
13. M. Benakli, H. Zheng, M. Gabay, Phys. Rev. **B 55**, 278 (1997).
14. M. Gabay, M. Benakli and W.M. Saslow, preprint (1997).
15. G. Uimin and A. Pimpinelli, Phys. Rev. **E 49**, 1123 (1994).
16. A. Pimpinelli, G. Uimin, and J. Villain, J. Phys. Condens. Matter **3**, 4693 (1991); J.L. Cardy, M.P.M. den Nijs, and M. Schick, Phys. Rev. **B 27**, 4251 (1983).
17. A.R. Day, T.C. Lubensky, A.J. McKane, Phys. Rev. **A 27**, 1461 (1983); see also D.R. Nelson in *Phase transitions and Critical Phenomena*, edited by Domb and Lebowitz (Academic Press, 1983), Vol.7, p. 89.
18. M. den Nijs, in Phase transitions and Critical Phenomena, edited by Domb and Lebowitz (Academic Press, 1988), Vol. 12, p. 219.